

Shipboard oceanographic fluorescence lidar development and evaluation based on measurements in Antarctic waters

K. Ohm^{*}, R. Reuter⁺, M. Stolze⁺ and R. Willkomm⁺

^{*} Alfred-Wegener-Institut für Polar- und Meeresforschung, D-27515 Bremerhaven, Germany
email: kohm@awi-bremerhaven.de

⁺ Carl von Ossietzky Universität Oldenburg, Fachbereich Physik, D-26111 Oldenburg, Germany
email: {r.reuter,willkomm}@las.physik.uni-oldenburg.de

ABSTRACT

The prototype of a shipboard lidar for oceanographic applications uses the 355 nm wavelength of a Nd:YAG-Laser to excite fluorescence of gelbstoff and chlorophyll in seawater. The lidar was installed on board the research vessel *Polarstern* at the end of 1996 during cruise ANT XIV/2. Measurements were carried out around the South Shetland Islands and in the Drake Passage between South America and the Antarctic Peninsula. Remotely measured depth profiles of the beam attenuation coefficient in the upper water column were derived from time resolved measurements of water Raman scattering. In the same way, depth profiles of gelbstoff and chlorophyll were derived from laser-induced fluorescence signals. These depth profiles were continuously taken while the ship was underway with a penetration depth of up to 40 m, depending on the detection wavelength and turbidity of the water. The data are compared with *in situ* fluorescence measurements. Limitations and advantages of remotely measured lidar profiles and *in situ* measurements with submerged probes are discussed.

1. INTRODUCTION

Except for the range of very low frequencies, visible light is the only portion of the electromagnetic spectrum that can be transmitted through water. Therefore, lidar remote sensing¹ allows a measurement of water column parameters with instruments installed on board ships^{2,3,4,5,6,7} or aircraft.^{8,9,10,11,12} Such measurements are mostly performed in a fluorosensing mode. Then an integration of the returned signal is done which is appropriate to derive data on phytoplankton pigments and other substances that are broadly dispersed in the upper water layers.

Efforts have also been spent on time-resolved measurements of elastically scattered or reflected laser pulses. The most prominent applications were to chart the water depth in shallow coastal areas by measuring the time lapse between signal returns from the sea surface and seafloor.^{13,14} With the same method but using a fast gateable camera as a detector, contrast enhanced images^{15,16} can be obtained from objects on the sea-

floor also in turbid waters where conventional imagery is not possible. Attempts have also been made to use time-resolved fluorescence signals for a classification of oil spills, which is based on the fluorescence decay time characteristics of oil.^{17,18,19,20}

Less effort has been spent to measure profiles of parameters of the water column that are relevant for oceanographic and marine biological studies. Seawater temperature profiles²¹ derived from the temperature dependent bandshape of water Raman scattering^{22,23,24} have not met the accuracy required for this parameter. More successful were the measurements of attenuation profiles from the intensity of elastic backscattering from particles^{25,26} and water Raman scattering²⁷ with airborne lidar. Both the attenuation coefficient and the gelbstoff concentration could be measured as profiles with 0.7 m resolution down to about 15 m water depth in coastal waters.²⁸

The successful operation of depth-resolving airborne lidar led to the decision to build a prototype for shipboard installation. This opens a way to gather remotely sensed profiles from the upper water layers over large areas of the open oceans, while the ship is underway and without any restriction to its operation (velocity, manoeuvring). An instrument was developed for installation on board the research vessel *Polarstern* (Fig. 1) of the Alfred Wegener Institute for Polar and Marine Research, Bremerhaven. The regular transects in the Atlantic Ocean between Europe and the Antarctic offer unique possibilities to employ a shipborne lidar on this vessel with the perspective to obtain underway data of bio-optical parameters that cannot be taken with other methods. Furthermore, operation on board a research vessel would allow to make use of a lidar over extended periods of time, which is of particular value within long-term monitoring programmes.

The instrument was originally designed in 1992-93 and applied for the first time during cruise ANT XI/1 of R.V. *Polarstern* in a transect through the Atlantic Ocean from Bremerhaven to Cape Town. The design and specifications of the prototype have been described in an earlier publication²⁹ and are only briefly summarized here.

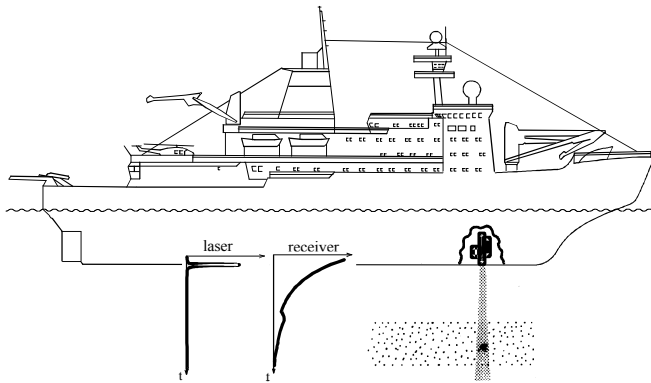


Fig. 1: Scheme of the installation on board R.V. Polarstern. Position of the instrument is at the keel of the ship at 11 m depth below the surface. The shadow of the ship protects the receiver field of view from daylight that would degrade the small signals from deeper layers.

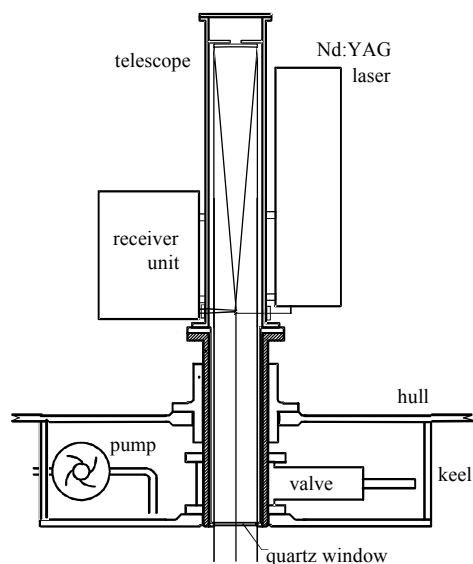


Fig. 2: Scheme of the lidar installed near the keel of the ship. The mechanical construction allows the installation of the system including the window without docking of the ship. To remove the lidar, the whole telescope set-up is lifted, and then the sliding valve is closed. Together with the gasket in the hull it forms a sluice that maintains the ship's security.

In this paper, we report on the progress that has been made since that time. The goal was to increase the sensitivity and dynamic range of the instrument, and the stability of its operation during long-term use on board the ship. Data from an expedition in the region of the Antarctic peninsula are presented where the lidar was continuously operated during 35 days. Some results obtained during that time are compared with depth profiles measured with conventional *in situ* sensors, and this allows to delineate the specific advantages and limitations of both methods.

2. THE INSTRUMENT

2.1 Layout and specifications

The lidar consists of a frequency-doubled and tripled Nd:YAG laser, a Newtonian telescope and a 12 channel receiver unit (Table 1). The telescope is the central element of the mechanical structure to which the laser and the detector unit are rigidly coupled to maintain a stable optical alignment (Fig. 2). The telescope is closed towards the water column by a quartz window. The telescope housing is pressure proved, with a tube thickness that corresponds to that of the ship's hull.

Laser:	Nd:YAG with Q switching, Quanta Systems model SYL A2
wavelengths:	used for excitation of:
532 nm (50 mJ)	532 nm elastic scattering 650 nm water Raman scattering 685 nm chlorophyll fluorescence via fucoxanthin absorption
355 nm (25 mJ)	355 nm elastic scattering 405 nm water Raman scattering 440 nm gelbstoff fluorescence 685 nm chlorophyll fluorescence
pulse length	< 1 ns
repetition rate	10 Hz
Telescope:	f/6 Newtonian, f = 1200 mm,
Spectrograph:	max. 12 discrete channels, wavelength selection with dichroic beamsplitters, interference filters
Detectors:	compact head-on photomultipliers UV... green: Hamamatsu R1635 red: Hamamatsu R1894
Signal recovery:	logarithmic amplification with Analog Modules model 382; digitisation with Tektronix model DSA 602 A

Table 1: Most relevant specifications of the instrument. The 532 nm laser wavelength was not used since the penetration depth into the water column at low gelbstoff concentration levels is about the same as with 355 nm.

2.2 Path of rays

To achieve a coaxial structure of the laser beam axis and telescope field of view, both the laser light and the telescope output pass through small windows at the side of the telescope housing. These windows are automatically closed in case of water intrusion into the telescope. To achieve the coaxial geometry, the laser

beam is folded into the central axis of the telescope with a 90° folding prism (Fig. 3).

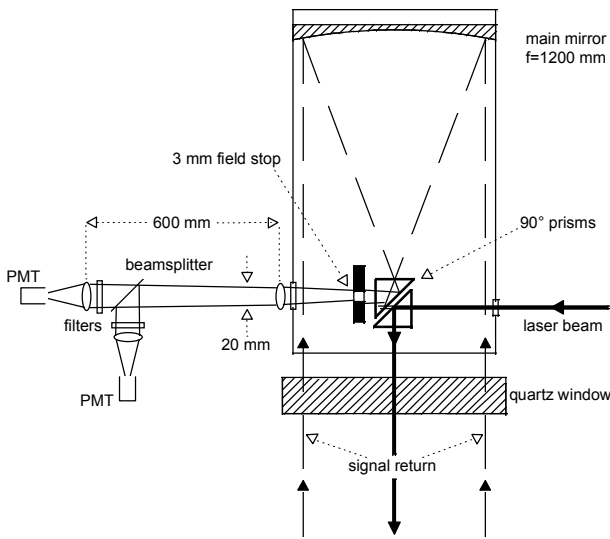


Fig. 3: Schematic drawing of the path of rays, not to scale.

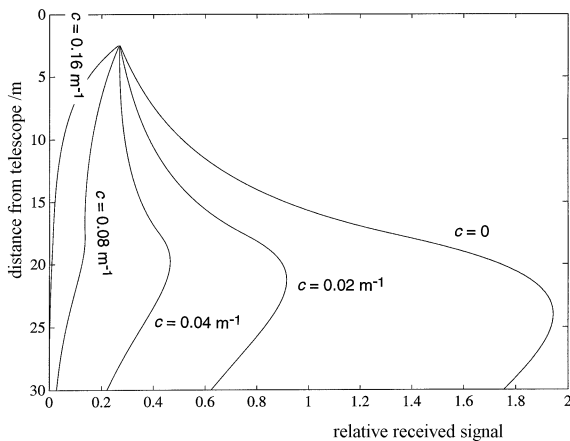


Fig. 4: Telescope sensitivity versus distance from its field stop with the attenuation coefficient c of the water as a parameter. Position of the field stop is chosen such that its image is at 30 m distance from the field stop of the telescope. Adopted from reference 31.

The secondary mirror of the Newtonian telescope is realized by another prism at about the same position, deflecting the signal return from the water column to the receiver unit. A 3 mm diameter field stop is close to this prism, at a short distance behind the focus of the main mirror of the telescope. The field stop is projected onto the cathodes of the photomultipliers, and this holds for the entire set of detection channels in the receiver unit because of their identical distance to the field stop. This symmetry of the detection channels cannot be achieved by other configurations of the optical set-up.³⁰

The diaphragms of the path of rays are designed in a way that all the light passing the field stop reaches the photomultipliers. Then the sensitivity of the set-up is a function of the distance from the telescope, that can be adapted to specific needs. In case of a hydrographic lidar high signal levels from short distances might lead to an overload of the detectors.³¹ It is the position of the field stop that determines the water depth of maximum sensitivity that has been chosen to 30 m for this instrument.

The shape of this sensitivity function of the receiver versus distance depends also on the attenuation coefficient of the water (Fig. 4). In principle, it could be tuned in a way that a close-to-constant shape over a considerable depth range would result for an attenuation coefficient of about 0.06 m^{-1} . However, these low values hold only in the blue part of the spectrum and in clear ocean waters. The attenuation coefficient near the 685 nm chlorophyll fluorescence band would be well above 0.4 m^{-1} also in clear waters. Therefore, in addition to the geometrical compression (Fig. 5) of the sensitivity function an additional logarithmic signal compression is always desirable. This is done with fast logarithmic amplifiers with a dynamic range of about 4 decades (Fig. 6). Their time response for the trailing edge of the photomultiplier output, which is of primary importance in this application, is about 5 ns per decade of input signal change. This is fast enough for a recovery of stratified layers in the upper water column.

Fig. 5: Experimental realisation of the geometrical compression of lidar signals. The curves display the signal return at the 405 nm water Raman scatter wavelength with 355 nm excitation, in a linear presentation, before and after correction for the telescope sensitivity versus water depth (or: elapsed time).

2.3 Electromagnetic interference

In the development phase of the lidar its use on board the ship was hampered by the occurrence of strong electromagnetic interference from the laser that severely degraded the photomultiplier output signals.

This can be seen in Fig. 7 that shows the signal return from water Raman scattering and chlorophyll fluorescence measured in 1993 during a first test of the instrument. The curves display the output signal of the logarithmic amplifiers. Taking into account that the signals should strictly fall over the trailing edge of these curves, the data are obviously degraded at output levels of the logarithmic amplifiers of less than about 0.2 V, and therefore useless over the largest part of their relevant dynamic range.

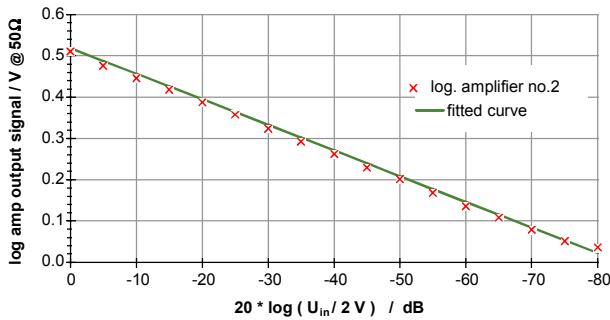


Fig. 6: Input/output characteristic of the logarithmic amplifiers. The crosses were obtained by calibration of the amplifier. The straight line is a fit used to interpret the lidar signals measured on board ship.

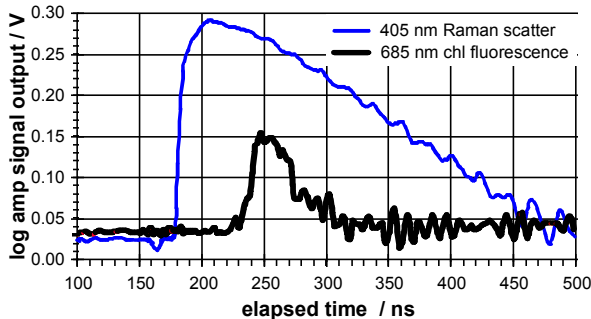


Fig. 7: Examples of signals degraded with noise, measured during the first test in the cruise ANT XI/1, October 1993. The curves display PMT signals from the given detection channels after logarithmic amplification, as an average of 128 single pulses. The chlorophyll fluorescence signal is much shorter than the water Raman return because of the higher attenuation coefficient, and hence lower lidar penetration depth, at the emission wavelength of chlorophyll fluorescence. The position of the leading edge of both signals on the abscissa is arbitrary.

The source of this electromagnetic interference was the switched high voltage of the Pockels cells of the laser. Therefore, a new housing of the laser was made with highly improved shielding characteristics against high frequency emission. In addition to this, the following measures were taken to reduce high frequency noise in the data:

- cables between laser head and laser power supply were shielded;
- signal lines between laser and receiver unit were realized with fiber optics;
- photomultiplier tubes were shielded with metal tubes;
- photomultiplier high voltage supplies were positioned closer to the photomultipliers, allowing for a short cable length between these components;

- the logarithmic amplifiers were individually powered with stabilized power supplies.

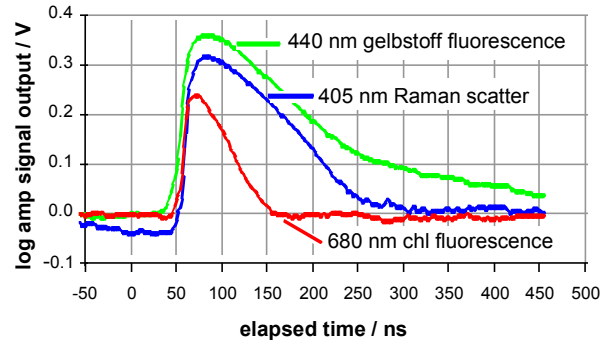


Fig. 8: Examples of signals measured during ANT XI/1, Dec. 1996. Better shielding against electromagnetic interference has led to a much lower noise level, thus allowing to use the logamp output over its entire dynamic range. The shape of the trailing edge of the signal is again due to the different attenuation coefficients at the given wavelengths.

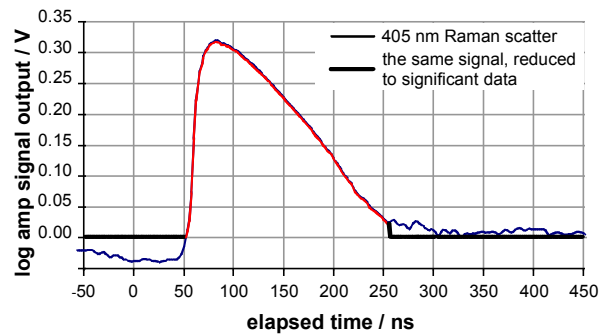


Fig. 9: To suppress noisy components in the signals, their bandshape is checked for plausibility. Noise at times before the leading edge is set to zero. The same is done at the end of the trailing edge, starting at a time where the signal is no longer decreasing.

These modifications resulted in a great improvement of the quality of the laser-induced signals from the water column (Fig. 8). The remaining noise at output levels below about 30 mV corresponding to the lower end of the dynamic range would still lead to erroneous profiles at these depths. During data evaluation, these signal contributions are rejected (Fig. 9).

3. EXPERIMENTAL RESULTS

3.1 Cruise ANT XI/2

Previous tests of the lidar were carried out on board R.V. *Polarstern* during long transects through the Atlantic Ocean between Europe and Cape Town, South Africa, or Ushuaia, South America. These routes led through the tropical deserts of the ocean, characterized

by very low biological activity and clear waters, and hence high penetration depth with lidar but small fluorescence signals.

During the expedition ANT XI/2 into the shelf regions of the Antarctic Peninsula, regions with much higher biological productivity were met. Fluorescence from the water column was stronger, but for the same reason the maximum penetration depth of the lidar was lower than in earlier campaigns and did not exceed about 15 to 20 m at the chlorophyll fluorescence wavelength. However, due to the increased sensitivity of the instrument the quality of these data is much better than in previous applications.

The cruise started from the Argentinean port Punta Quilla and led through the Drake Passage into the region of the South Shetland Islands. In the period of 16 November to 22 December 1996, hydrographic data were measured over a meshed grid of stations nearby Elephant Island (Figs. 10, 11). The measurements included depth profiles of temperature, salinity and chlorophyll fluorescence, and water sampling for a fluorometric analysis in the laboratory.

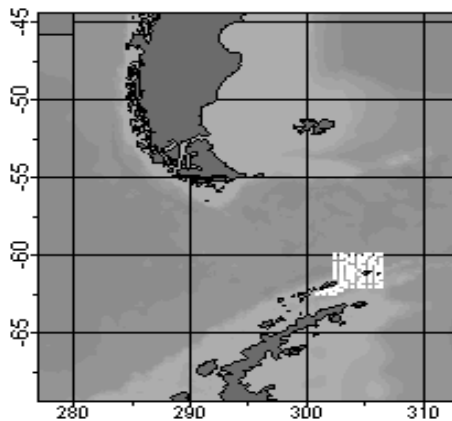


Fig. 10: Geographical position of the station grid investigated in the expedition ANT XVI/2 of R.V. Polarstern, 16.11.-22.12.97

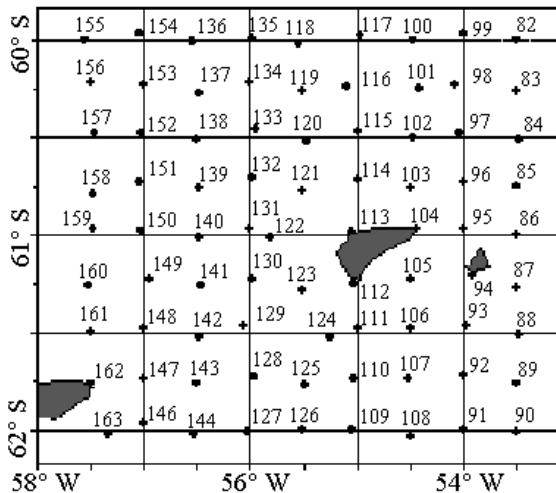


Fig. 11: Meshed grid in the region of Elephant Island, shown as white box in Fig. 9. The grid consists of 81 stations as indicated, at distances of about 15 nautical miles.

3.2 Lidar measurements

During the survey the lidar was continuously operated. The signals from 128 single shots of the laser, fired with a repetition rate of 10 Hz, were averaged. This yields a better signal-to-noise ratio, and a higher dynamic resolution than the 8 bit of the transient digitizer. Examples of these data are shown in Figs. 8 and 9. Records derived in this way were obtained in intervals of five minutes, leading to a depth profile at distances of one nautical mile while the ship was underway between the stations.

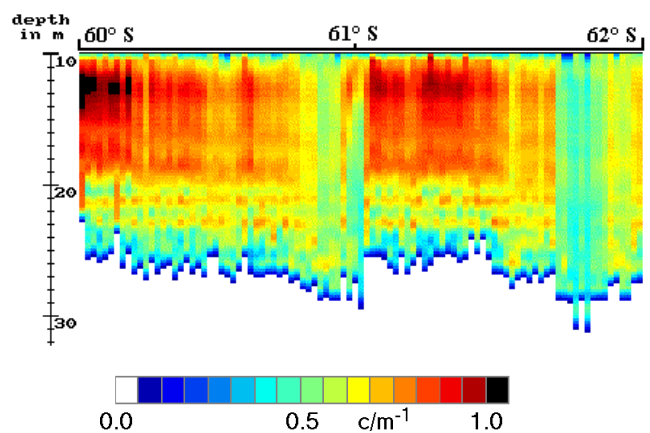


Fig. 12: Sum of the attenuation coefficients $c(355 \text{ nm}) + c(405 \text{ nm})$ given in m^{-1} , measured with lidar along a transect between stations 100 and 108 on latitude $54^{\circ}30' \text{W}$ (Figs. 9 and 10). Positions of stations are marked, where depth profiles were taken with in situ probes. The unsteady behaviour of the data at depth is due to the variable penetration depth of the lidar, and hence reflects the local values of the attenuation coefficient.

As an example of this data set, the depth profiles measured on a north-south transect between stations 100 and 108 are shown in Fig. 12. The graph displays the sum of the attenuation coefficients at the wavelengths of laser excitation and water Raman scatter $c(355 \text{ nm}) + c(405 \text{ nm})$ in absolute units.

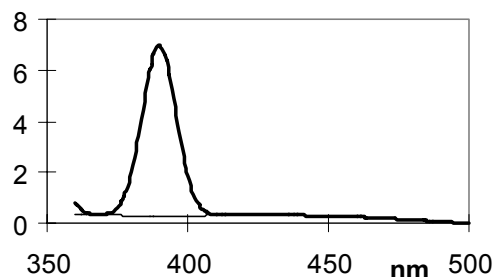


Fig. 13: Emission spectrum, with 341 nm excitation of a water sample taken from 20 m depth at station 108, measured with a Perkin Elmer LS50 spectrofluorometer. The curve is corrected for the spectral sensitivity of the instrument. The peak at 386 nm is water Raman scattering, the weaker signals at higher wavelengths are gelbstoff fluorescence.

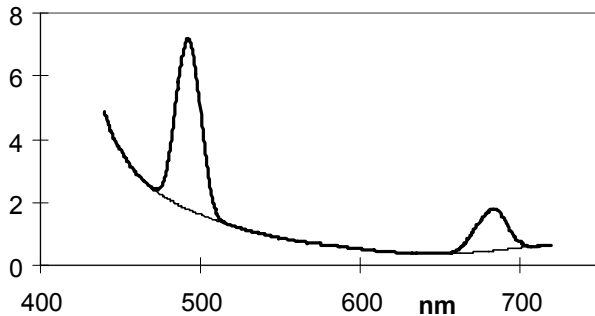


Fig. 14: Same as in Fig. 13, but with 420 nm excitation. The peak at 490 nm is water Raman scatter, chlorophyll fluorescence is at 685 nm. The baseline below these bands is an artefact due to stray light from the excitation monochromator, caused by a defective grating. In the data given in Fig. 13, the stray light was suppressed with an 341 nm interference filter in the excitation raypath.

The attenuation coefficient hardly ever exceeds values of about 1 m^{-1} . The main reason for the dynamics of this parameter is the variability of the phytoplankton abundance. Gelbstoff, which might affect the attenuation coefficient as well, has a weaker influence on this parameter because of its low concentration in this region. Although photometric measurements were not made on board the ship, small values of the absorption coefficient of gelbstoff are estimated from its low fluorescence signal (Fig. 13) compared with the fluorescence of phytoplankton (Fig. 14).

The distribution of phytoplankton along the same transect, derived from its fluorescence emission at 685 nm wavelength, is shown in Fig. 15. The close relationship between attenuation and chlorophyll fluorescence is obvious from these data.

3.3 Comparison of lidar and *in situ* data

When the ship was on stations, depth profiles were made with a CTD probe equipped with an *in situ* fluorometer (backscat fluorometer, Haardt, Germany) for continuous chlorophyll and gelbstoff fluorescence measurements in the water column. A comparison of these data with lidar profiles is useful for an understanding of the advantages and limitations of both methods.

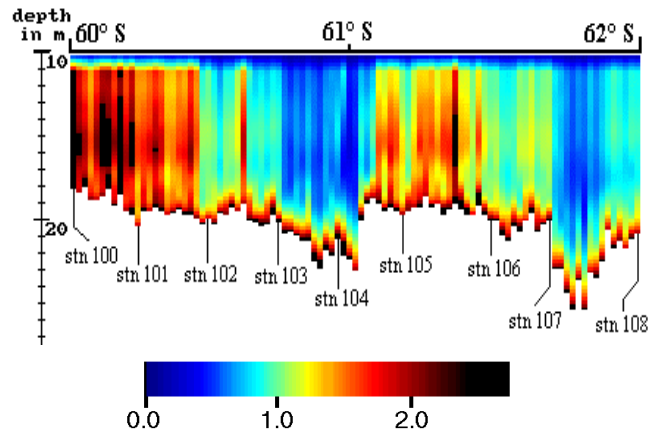


Fig. 15: Same as in Fig. 12, but depth profiles of chlorophyll fluorescence at 685 nm in arbitrary units, normalized to water Raman scattering.

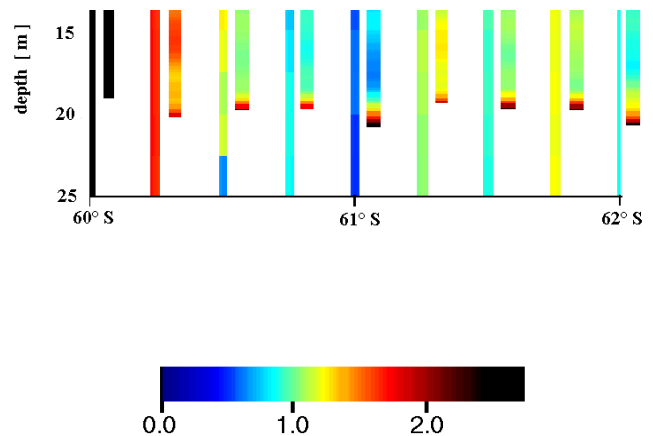


Fig. 16: Comparison of *in situ* profiles of chlorophyll fluorescence (bars from 10 to 25 m depth) and lidar depth profiles (thicker bars with variable maximum depth).

For this purpose, nine lidar records of chlorophyll fluorescence measured while the ship was on a station are selected from the data set and compared with the results of *in situ* probing (Fig. 16). In principle, the dynamics of chlorophyll fluorescence between stations is well represented by both methods. Also, the variations versus depth are identically found in the data. To describe this in more detail, the dependence of lidar and *in situ* data is calculated at intervals of one meter for the entire data set at these stations (Fig. 17). This shows that the lidar profiles are in good agreement with the *in situ* data at depths of about 12 to 18 m. In the near field of the lidar, e.g. at depth of 11 to 12 m just below the ship's hull, the data are inaccurate because of the strong gradient of the telescope sensitivity function there. At depths of more than 19 m that correspond to the maximum penetration depth of the lidar, the error increases strongly because of small signal intensities.

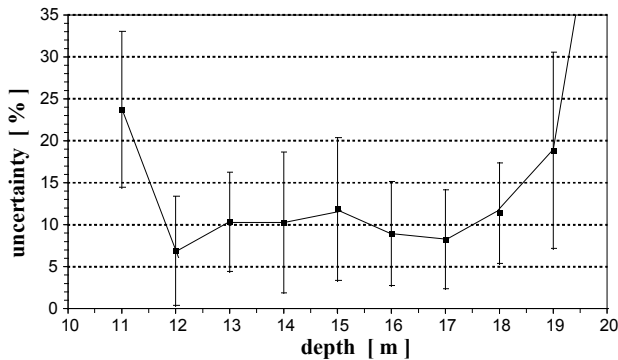


Fig. 17: Uncertainty of the lidar depth profiles of chlorophyll fluorescence from stations 100 to 108, with the *in situ* profiles from the same stations taken as the reference. Error bars correspond to the standard deviation of the mean values.

4. CONCLUSION

Although identical in principle, air- and shipborne lidars face different problems in practice. If carried by an aircraft some hundreds of metres above the sea surface the time lapse between sending out the laser pulse and the return of the signal from the water column is about one microsecond. This is sufficient to avoid electromagnetic interference from the laser power electronics to the sensitive detectors and signal amplifiers. This is not the case for a lidar system on board a ship where signals have to be registered in the near-field of operation, that is within a few nanoseconds following the laser pulse emission. Modifications of the instrument performed since its first use on board the ship have led to a great improvement of the signal-to-noise ratio. This makes it possible to interpret the signal return over a dynamic range of three decades, corresponding to a penetration depth in the upper water column of about 6 attenuation length.

The data obtained in the cruise ANT XVI/2 of R.V. *Polarstern* show that, in addition to seawater attenuation and gelbstoff, profiles of chlorophyll fluorescence can be measured in the upper water column. This is of high interest in regions with enhanced biological productivity where phytoplankton is present near the surface. In these applications, a lidar should be installed closer to the sea surface, which was not feasible on board R.V. *Polarstern*.

On the other hand, oligotrophic regions of the open oceans are characterized by very low biological productivity in the surface mixed layer. Phytoplankton growth is there at depths of about 50 to 100 m, that is just below the mixed layer where stratification takes place.³² This would exceed the depth range that can be reached with lidar, especially if chlorophyll fluorescence is of primary interest since the attenuation coefficient

of pure water is high at this wavelength. However, elastic (Mie) scattering measured in the blue or near ultraviolet spectral range where water shows good transparency would allow to map deep-lying plankton layers. Such measurements should be attempted with this instrument in a next step of its development.

The results show further the value of profiles derived while the ship is underway, compared to the same parameters measured with *in situ* probes on stations. Both methods yield consistent results at stations (Fig. 16), but the data found there are not sufficient to sample the „true“ distribution of phytoplankton, even at distances of only 15 nautical miles between the stations. Patchiness of plankton distributions even at smaller scales is typical in the ocean. For example, the high chlorophyll fluorescence between stations 102-103 and 105-106 is easily detected with lidar.

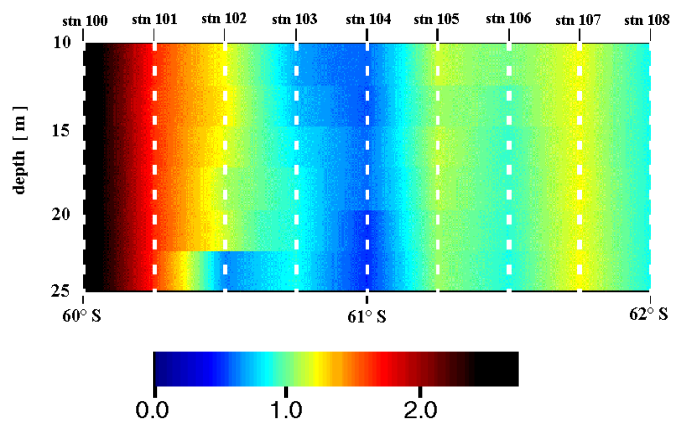


Fig. 18: Profiles at stations 100-108 taken with the *in situ* fluorometer are interpolated with Surfer 6.01 (Golden Software, Inc.), a programme often used in oceanography for this purpose. Locations of depth profiles are marked with white dashed lines. See Fig. 15 for a comparison with the results of continuous sampling with lidar.

The higher information content of lidar data is particularly evident if the *in situ* profiles measured on stations are used for an interpolation of the plankton distribution in the region. The use of an interpolation programme would lead to the diagram shown in Fig. 18, and hence to erroneous results.

5. ACKNOWLEDGEMENTS

This work was financially supported by the Federal Ministry of Research and Technology, Bonn, within the frame of the Eureka project Euomar. We are grateful to Horst Harms who was engaged in the improvement of the lidar and also took part in the expedition ANT XIV/2. We wish to thank the captain and the crew of R.V. *Polarstern* for their support during the experi-

ments on board the ship. We are grateful to Mme. Madeleine Godefroy and an anonymous reviewer; their comments were very helpful in improving the manuscript.

6. REFERENCES

- ¹ R.M. Measures, „Laser Remote Sensing. Fundamentals and Applications“, Wiley, New York, 510 pp, 1984
- ² W.M. Houghton, R.J. Exton and R.W. Gregory, „Field investigation of techniques for remote laser sensing of oceanographic parameters“, *Remote Sensing of Environment*, 13, 17-32, 1983
- ³ A. Dudelzak, S.M. Babichenko, L.V. Poryvkina and K. Saar, „Total luminescent spectroscopy for remote laser diagnostics of natural water conditions“, *Applied Optics*, 30, 453-458, 1991
- ⁴ A.M. Chekalyuk, A.A. Demidov, V.V. Fadeev and M.Yu. Gorbunov, „Lidar monitoring of phytoplankton and organic matter in the inner seas of Europe“, *EARSel Advances in Remote Sensing*, 3(3), 131-139, 1995
- ⁵ L. Alberotanza, P.L. Cova, C. Ramasco, S. Vianello, M. Bazzani, G. Cecchi, L. Pantani, V. Raimondi, P. Ragnarson, S. Svanberg and E. Wallinder, „Yellow substance and chlorophyll measurements in the Venice Lagoon using laser-induced fluorescence“, *EARSel Advances in Remote Sensing*, 3(3), 102-111, 1995
- ⁶ S.M. Babichenko and L. Poryvkina, „Application of tuneable lidars of FLS series in marine applications“, paper included in this volume.
- ⁷ R. Barbini, F. Colao, R. Fantoni, A. Palucci and S. Ribezzo, „The ENEA mobile lidar fluorosensor equipment for marine campaigns“. In: *Proceedings of the 3rd EARSel Workshop on Lidar Remote Sensing of Land and Sea*, Tallinn 1997, S. Babichenko and R. Reuter (editors). Published by EARSel, Paris, in print.
- ⁸ H.H. Kim, „New algae mapping technique by the use of an airborne laser fluorosensor“, *Applied Optics*, 12, 454-462, 1973
- ⁹ F.E. Hoge and R.N. Swift, „Delineation of estuarine fronts in the German Bight using airborne laser-induced water Raman backscatter and fluorescence of water column constituents“, *International Journal of Remote Sensing*, 3, 475-495, 1982
- ¹⁰ M.P.F. Bristow, D. Bundy, C.M. Edmonds, P.E. Ponto, B.E. Frey and L.F. Small, „Airborne laser fluorosensor survey of the Columbia and Snake rivers: simultaneous measurements of chlorophyll, dissolved organics and optical attenuation“, *International Journal of Remote Sensing*, 6, 1707-1734, 1985
- ¹¹ R. Reuter, D. Diebel and T. Hengstermann, „Oceanographic laser remote sensing: measurement of hydrographic fronts in the German Bight and in the Northern Adriatic Sea“, *International Journal of Remote Sensing*, 14, 823-848, 1993
- ¹² W. Milchers, S. Patsayeva, R. Reuter and R. Willkomm: „Airborne laser fluorosensing of maritime parameters: application of geostatistics“, paper included in this volume.
- ¹³ G.D. Hickman and J.E. Hogg, „Application of an airborne pulsed laser for near-shore bathymetric measurements“, *Remote Sensing of Environment*, 1, 47, 1969
- ¹⁴ O. Steinvall, H. Klevebrant, J. Lexander and A. Widen, „Laser depth sounding in the Baltic Sea“, *Applied Optics*, 20, 3284, 1981
- ¹⁵ F. Ahrenberg, S. Harsdorf, J. Niehues and R. Reuter, „Contrast enhanced imaging in the sea: application of the optical transfer function for image reconstruction“. In: *Proceedings of the 3rd EARSel Workshop on Lidar Remote Sensing of Land and Sea*, Tallinn 1997, S. Babichenko and R. Reuter (editors). Published by EARSel, Paris, in print.
- ¹⁶ S. Harsdorf, M. Janssen, R. Reuter and B. Wachowicz, „Submarine fluorescence lidar for environmental monitoring“. In: *Proceedings of the 3rd EARSel Workshop on Lidar Remote Sensing of Land and Sea*, Tallinn 1997, S. Babichenko and R. Reuter (editors). Published by EARSel, Paris, in print.
- ¹⁷ R.M. Measures, H.R. Houston and D.G. Stephenson, „Laser-induced fluorescence decay spectra - a new form of environmental signature“, *Optical Engineering*, 13, 444-450, 1974
- ¹⁸ D.M. Rayner and A.G. Szabo, „Time-resolved laser fluorosensors laboratory study of their potential in the remote characterization of oil“, *Applied Optics*, 17, 1624-1630, 1978
- ¹⁹ D. Diebel, T. Hengstermann and R. Reuter, „Classification of oil types with time-resolved fluorescence signal detection: a computer model study“. In: *Remote Sensing of Pollution of the Sea*, R. Reuter and R.H. Gillot (editors), Commission of the European Communities, Joint Research Centre - Ispra Establishment, S.P.I. 87.46, pp. 266-280, 1987
- ²⁰ P. Camagni, A. Colombo, C. Koechler, N. Omenetto and G. Rossi, „Fluorescence response of mineral oils: spectral yield vs. absorption and decay time“, *Applied Optics*, 30, 26-35, 1991.

- ²¹ D.A. Leonard, B. Caputo and F.E. Hoge, „Remote sensing of subsurface water temperature by Raman backscattering“, *Applied Optics*, 18, 1732-1745, 1979.
- ²² J.R. Scherer, M.K. Go and S. Kint, „Raman spectra and structure of water from -10 to 90°“, *The Journal of Physical Chemistry*, 78, 1304-1313, 1974
- ²³ C.H. Chang and L.A. Young, „Seawater temperature measurement from Raman spectra“, AVCO Everett Research Laboratory, Research Note 960, 82 pp., Jan. 1974
- ²⁴ A.Yu. Bekkiev, T.A. Gogolinskaya and V.V. Fadeev, „Simultaneous determination of the temperature and salinity of sea water by laser Raman spectroscopy“, *Sov. Phys. Dokl.*, 28(8), 639-641, 1983
- ²⁵ B. Billard, R.H. Abblot and M.F. Penny, „Airborne estimation of sea turbidity parameters in an airborne laser hydrographic system“, *Applied Optics*, 25, 2080-2088, 1986
- ²⁶ F.E. Hoge, C.W. Wright, W.B. Krabill, R.R. Buntzen, G.D. Gilbert, R.N. Swift, J.K. Yungel and R.E. Berry, „Airborne lidar detection of subsurface oceanic scattering layers“, *Applied Optics*, 27, 3969-3977, 1988
- ²⁷ F.E. Hoge and R.N. Swift, „Airborne detection of oceanic turbidity cell structure using depth-resolved laser-induced water Raman backscatter“, *Applied Optics*, 22, 3778-3786, 1983
- ²⁸ D. Diebel-Langohr, T. Hengstermann and R. Reuter, „Water depth resolved determination of hydrographic parameters from airborne lidar measurements“. In: *Marine Interfaces Ecohydrodynamics*, J.C.J. Nihoul (editor), (Amsterdam: Elsevier), pp. 591-602, 1986
- ²⁹ R. Reuter, R. Willkomm, G. Krause and K. Ohm, „Development of a shipboard lidar: Technical layout and first results“, *EARSeL Advances in Remote Sensing*, 3(3), 15-25, 1995
- ³⁰ W. Lüdecker, K.P. Günther and H.G. Dahn, „Comparison of different detection set-ups for laser-induced fluorescence monitoring of vegetation“, *EARSeL Advances in Remote Sensing* 3(3), 32-41, 1995
- ³¹ K. Ohm and R. Willkomm, „Collecting performance of a lidar telescope at short distance“, *EARSeL Advances in Remote Sensing* 3(3), 2-31, 1995
- ³² K.H. Mann and J.R.N. Lazier, „Dynamics of Marine Ecosystems. Biological - physical interactions in the oceans“, Blackwell Scientific Publications, 1991